ADVANCED FUNCTIONAL MATERIALS

FULL PAPER

DOI: 10.1002/adfm.200601117

Large-Size Bulk and Thin-Film Stilbazolium-Salt Single Crystals for Nonlinear Optics and THz Generation**

By *Zhou Yang*,* *Lukas Mutter*, *Marcel Stillhart*, *Blanca Ruiz*, *Shanmugam Aravazhi*, *Mojca Jazbinsek*, *Arno Schneider*, *Volker Gramlich*, and *Peter Günter*

We present new stilbazolium salt DSTMS (4-*N*,*N*-dimethylamino-4′-*N*′-methyl-stilbazolium 2,4,6-trimethylbenzenesulfonate) with both high second-order nonlinear optical properties and very favorable crystal growth characteristics. We are able to obtain very large area bulk single crystals of more than $3 \times 3 \times 0.2$ cm^3 with a high optical quality without using seed crystals by using low-temperature solution growth. We also demonstrate the growth of single crystalline thin films of DSTMS with an area of up to 6×5 mm^2 and a thickness between 5–30 μm. Nonlinear optical measurements reveal that DSTMS possesses large nonlinear optical susceptibilities with $\chi_{111}^{(2)} = (430 \pm 40)$ pm V^{-1} at 1.9 μm. Highly efficient generation of broadband THz waves with THz electric field strengths of more than 4 kV cm^{-1} using 160 fs laser pump pulses at a wavelength $\lambda = 1.45$ μm and DSTMS crystals has been demonstrated.

1. Introduction

During the last two decades, there have been intensive research efforts in exploring and developing second-order nonlinear optical (NLO) materials for applications such as frequency conversion, electro-optic modulation and optical parametric oscillation,[1–4] and more recently, THz generation and detection.[5] Compared with inorganic materials, molecular organic materials have been of considerable interest due to their large nonlinear optical properties, ultrafast response times and almost unlimited design possibilities.[6,7] Among them, organic crystals based on the charged chromophores and strong Coulomb interaction have several advantages over non-ionic species, such as large molecular nonlinearity or first-order hyperpolarizability (β), long-term stability and a higher tendency to override the dipole-dipole interactions and thus form non-centrosymmetric macroscopic packing.[8,9] For example, the organic salt crystal, 4-*N*,*N*-dimethylamino-4′-*N*′-methyl-stilbazolium tosylate (DAST) is one of the best nonlinear optical materials with large second-order nonlinear optical susceptibilities $\chi_{111}^{(2)} = (2020 \pm 200)$ pm V^{-1} at 1.3 μm and $\chi_{111}^{(2)} = (420 \pm 110)$ pm V^{-1} at 1.9 μm due to the good alignment of the chromophores in the crystal.[10,11] DAST consists of a positively charged nonlinear optical chromophore stilbazolium and a negatively charged tosylate anion. The counter-ion tosylate is used in order to override the preferred antiparallel crystallization of the chromophores. Up to date, DAST is the only commercially available organic nonlinear optical crystal.[12] However, its growth is still a challenge and there are many groups investigating the growth of bulk and thin films of DAST.[13–16] For example, one of the challenges is to reduce the growth time needed to obtain high optical quality DAST, which takes several weeks for crystals with dimensions exceeding 1 cm^3.[12]

Although DAST shows large electro-optic effects, the development of new organic crystals with larger electro-optic coefficients and (or) faster and easier crystal growth procedure is an important challenge for future applications. It has already been demonstrated that varying the counter-ion to optimize the crystal packing and orient the dipoles as parallel as possible is an effective molecular engineering strategy to develop ionic organic crystals with non-centrosymmetric structure.[17–20] Using this approach, we have reported the synthesis and crystal growth of DSNS (4-*N*,*N*-dimethylamino-4′-*N*′-methyl-stilbazolium 2-naphthalenesulfonate)—a promising DAST derivative with perfectly aligned chromophores, leading to a 50 % higher nonlinearity in the crystalline powder than DAST.[21] However, only very small crystalline needles of DSNS with a diameter of less than 100 μm could be grown.[21] We are therefore looking for a new highly nonlinear compound that could easily give crystals of large area suitable for bulk and thin film applications. We present here a new promising DAST derivative (see Scheme 1) with high solubility that is more than two times the one of DAST in methanol at the same temperature. We show that organic crystals with similar nonlinear optical properties as DAST are feasible with a considerably faster crystal growth rate and much better perspectives for growing single crystalline thin films for integrated optics.

[*] Dr. Z. Yang, L. Mutter, M. Stillhart, B. Ruiz, Dr. S. Aravazhi, Dr. M. Jazbinsek, Dr. A. Schneider, Prof. P. Günter
Nonlinear Optics Laboratory, Institute of Quantum Electronics
ETH Zurich, 8093 (Switzerland)
E-mail: nlo@phys.ethz.ch
Prof. V. Gramlich
Laboratory of Crystallography, Department of Materials
ETH Zurich, 8093 (Switzerland)

[**] This work has been supported by the Swiss National Science Foundation.

ADVANCED FUNCTIONAL MATERIALS

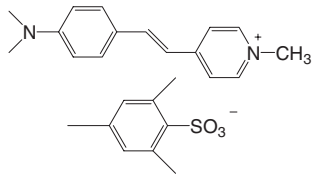

Scheme 1. Molecular structure of DSTMS.

2. Results and Discussion

2.1. Synthesis and Characterization

4-*N*,*N*-dimethylamino-4′-*N*′-methyl-stilbazolium 2,4,6-trimethylbenzenesulfonate (DSTMS) was synthesized according to the procedure described previously.[18] The product was purified by recrystallization (three times) from methanol before characterization by NMR and elemental analysis. It was easy to obtain orange color hydrate centrosymmetric crystals in the presence of water and the water could be removed by heating above 100 °C for 1–2 h.

DSC and TGA analyses have shown that the melting point of DSTMS is (258 ± 1) °C and begins to decompose at around 250 °C.

DSTMS can be well dissolved in some strong polar solvents such as methanol, DMF and DMSO etc.. However, DMF and DMSO are not well suited for crystal growth because of their high boiling points. Therefore methanol was chosen as the solvent for the growth of DSTMS crystals. Figure 1 shows the solubility curve for DSTMS in methanol solution in comparison with DAST. The solubility at a temperature T was measured by saturating the solution at a higher temperature (about 5 °C above T), slowly cooling it in the presence of a precipitated solid to maintain equilibrium, and then analyzing the solution at the temperature T. The solubility of DSTMS is around two times as large as the one found in DAST in methanol at the same temperature in the temperature range of interest. The large difference in the solubility can mainly be attributed to the different structure of counter-anions—the solubility of 2,4,6-trimethyl-benzenesulfonate that possesses three methyl groups should be higher than that of tosylate that possesses only one methyl group.

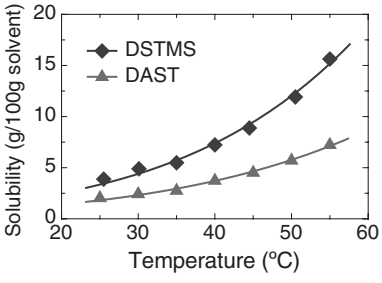

Figure 1. Solubility/temperature curves of DSTMS and DAST in methanol. The solid curves are according to equation (1) with $\Delta H = (81 \pm 4)$ kJ mol^{-1} and $\Delta S = (170 \pm 10)$ J mol^{-1} K^{-1}) for DSTMS and $\Delta H = (74 \pm 3)$ kJ mol^{-1} and $\Delta S = (140 \pm 10)$ J mol^{-1} K^{-1} for DAST.

The temperature dependence of the solubility of a dilute solution, considering that the solute dissolves into two ions, can be described by[22]

$$x_s = \exp\left(\frac{\Delta S}{2R}\right)\exp\left(-\frac{\Delta H}{2RT}\right) \quad (1)$$

where x_s is the molar fraction of the solute at saturation, $R = 8.314$ J mol^{-1} K^{-1} is the gas constant, and T the temperature in K. The thermodynamic parameters ΔS and ΔH are the changes of the entropy and enthalpy when dissolving the solute. The measured solubility S (in g of solute per 100 g of solvent) is related to the molar fraction of the solute x_s as $S = 100\,(M_{solute}/M_{solvent})\,x_s/(1-x_s)$, where $M_{solute/solvent}$ is the molecular mass of the solute/solvent. Analyzing the solubility data using Equation 1 shows that both ΔS and ΔH are larger for DSTMS compared to DAST and can be considered constant in the temperature region of interest (see Fig. 1).

An important parameter that affects the growth rate in solution-growth systems is the driving force for crystallization $\Delta\mu = \mu_s - \mu_c$, defined by the difference between the chemical potential of the solute in the solution μ_s and in the crystalline phase μ_c. If we increase the concentration of the solute in the solution from x_s to x_s', the driving force can be expressed simply as $\Delta\mu = 2RT\,(\ln x_s' - \ln x_s)$[22] or with the level of supersaturation $\sigma = (x_s' - x_s)/x_s$ as $\Delta\mu = 2RT\ln(1+\sigma) \approx 2RT\sigma$. Supersaturation in our system is achieved by lowering the temperature of the saturated solution from T' to T. Using Equation 1 and considering small $\Delta T = T' - T$ we obtain for the driving force $\Delta\mu = (\Delta T/T)\,\Delta H$. Therefore, an increased driving force for crystallization of DSTMS compared to DAST is expected due to larger ΔH when lowering the temperature of the saturated solution by ΔT.

2.2. Crystal Growth and X-Ray Crystallographic Study

It was found that DSTMS nucleated very easy and fast. From the recrystallization procedure to purify the material we were already able to get optical quality thin single-crystalline plates with dimensions of $5 \times 5 \times 0.3$ mm^3. Contrary to DAST, we are able to easily grow large bulk DSTMS crystals without a seed given the improved growth characteristics of the latter. Slow cooling technique was adapted for the growth of bulk crystals.[20] First we prepared saturated solution of DSTMS in methanol at 35–40 °C. Spontaneous nucleation could be observed after cooling down the saturated solution. Then we increased the temperature to dissolve most of the nuclei and made sure that only one or two nucleated crystals remained undissolved. After that, large crystals with very good optical quality for optical measurements could be grown by slow cooling the solution at a rate of 0.2–0.3 °C day^{-1}. Typically the crystals first appear as red thin plates and continue to grow preferentially along the edges in all directions. DAST, on the other hand, prefers to grow only along the direction of the polar axis [–100].[16] Using this self-nucleating method we can eliminate the defects introduced by seeds and omit the process of selecting, processing

and fixing the seed crystals. Large single crystal with dimensions of $33 \times 33 \times 2$ mm^3 have been grown by this method in a period of eight weeks (Fig. 2a). Experiments show that we can grow high quality single crystals of DSTMS with surface

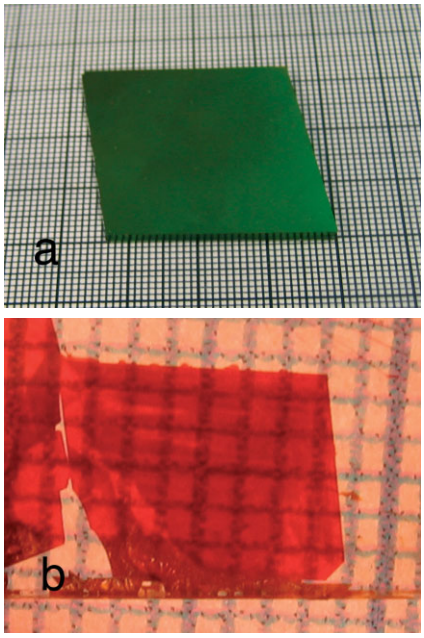

Figure 2. a) DSTMS bulk crystal (size $33 \times 33 \times 2$ mm^3), the large surface is the (001) face. b) DSTMS thin film crystal (size $6 \times 5 \times 0.03$ mm^3) grown by the capillary method.

area of about 1 cm^2 in 2 weeks, thus much faster than that of DAST (4–6 weeks).

For integrated optics applications the possibility of growing single crystalline thin films is very attractive. In view of the good quality of the thin plates spontaneously grown from DSTMS solution, we have done experiments on thin film growth by the capillarity method.[16] In this method, two glass plates are placed together in solution and capillary force pulls up the liquid. The slow evaporation of the solvent allows for growth. We have obtained single crystalline thin films with an area of up to 6×5 mm^2 and a thickness between 5–30 μm (Fig. 2b).

The crystallographic structure of DSTMS was determined via X-ray analysis of single crystals. The data obtained are listed in Table 1 and compared to the one of DAST. The crystal packing, which belongs to the monoclinic space group *Cc* (point group m, $Z = 4$), is shown in Figure 3. Crystallographic data show that beside the Coulombic interactions between the cation and anion parts, hydrogen bonds between the sulfonic oxygen atoms and double-bond hydrogen atoms also play a role in crystal packing and chromophores orientation. Figure 4 shows the hydrogen-bonded network formed by two kinds of C–H···O hydrogen bonds between the cation layers and the anion layers with H···O distances of about 2.49 Å and 2.44 Å, respectively.

Table 1. Crystallographic and other data of DSTMS and DAST crystals. θ_{lz} is the angle between the long axis of the cation chromophores and the polar axis of the crystal, T_m the melting temperature and $\chi_{111}^{(2)}$ the element of the second-order nonlinear optical susceptibility tensor for second-harmonic generation at fundamental wavelength of 1.9 μm.

Sample	DSTMS	DAST
Formula	$C_{25}H_{30}N_2O_3S$	$C_{23}H_{26}N_2O_3S$
FW	438.57	410.52
Crystal system	Monoclinic	Monoclinic
Space group	Cc	Cc
a(Å)	10.266	10.365
b(Å)	12.279	11.322
c(Å)	17.963	17.892
α(°)	90	90
β(°)	93.04	92.24
γ(°)	90	90
V(Å^3)	2261.2	2099.7
θ_z(°)	23	20
T_m(°C)	258 ± 1	256 ± 1
$\chi_{111}^{(2)}$ (pm/V)	430 ± 40	420 ± 110

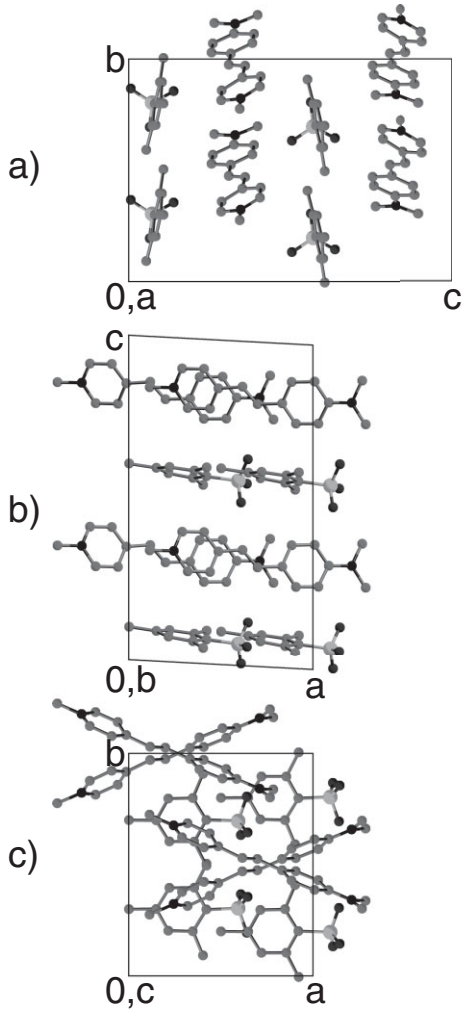

Figure 3. Crystal packing of DSTMS projected along the crystallographic axes *a* (a), *b* (b), and *c* (c). The mirror symmetry plane is perpendicular to the *b*-axis. The chromophores make an angle of approximately 23° with respect to the polar *a*-axis (c).

ADVANCED FUNCTIONAL MATERIALS

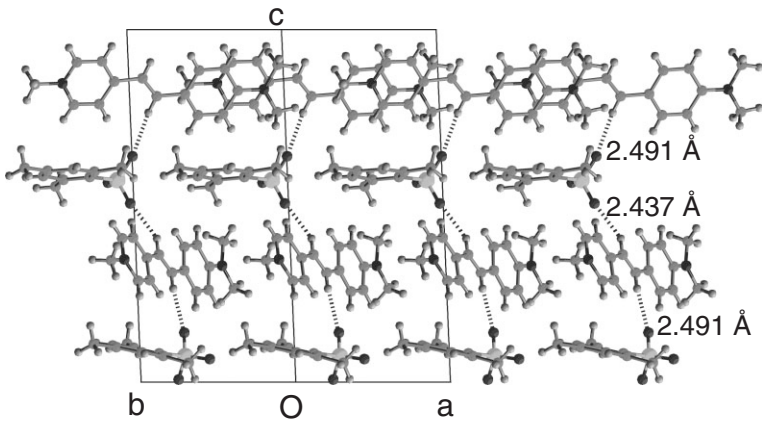

Figure 4. Crystal packing diagram of DSTMS projected along the [110] crystallographic vector. The molecules are linked by Coulombic interactions between the ionic parts and by hydrogen bonds that are indicated by dotted lines.

2.3. Linear Optical Properties

Light transmission spectra of DSTMS were measured for light polarized along the polar *a*-axis, which is most interesting for applications, and for light polarized along the crystallographic *b*-axis. For this measurement, an as-grown *c*-plate sample with a thickness of 0.77 mm was optically polished. The sample transmission was measured using a Perkin-Elmer Lambda 9 spectrophotometer along the two main axes and is shown in Figure 5. Three absorption bands observed in the infrared region at about 1.2, 1.4, and 1.7 μm correspond to overtones of the C–H stretching vibrations and have also been observed in DAST.[11]

The refractive indices we have measured at the telecommunication wavelength of 1.55 μm by an interferometric technique.[3] DSTMS crystals are strongly anisotropic with refractive index of $n_a = 2.07 \pm 0.05$ along the polar *a* axis, and $n_b = 1.64 \pm 0.05$ along the *b* axis. Using the refractive index data, we calculated the optical absorption from the transmission measurement of Figure 5 by considering Fresnel losses due to multiple reflections at the crystal surfaces. We determined the absorption constants at 1.55 μm as $\alpha_a = (0.6 \pm 0.1)$ cm^{-1} and $\alpha_b = (0.5 \pm 0.1)$ cm^{-1} for light polarized along the *a*-axis and along the *b*-axis respectively. Low optical loss measured shows that the sample has good optical surfaces and is free from scattering centers within the crystal.

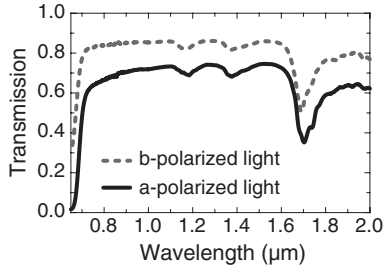

Figure 5. Transmission spectra of 0.77 mm thick DSTMS crystal for light polarized along the polar *a*-axis (solid curve) and along the crystal *b*-axis (dashed curve).

2.4. Nonlinear Optical Properties

The nonlinear optical properties were measured by the standard Maker Fringe technique.[23] The first Stokes line at 1907 nm generated in a high pressure Raman cell filled with H_2 and pumped with a Q switched Nd:YAG at 1064 nm (pulse length of 7 ns) was used as fundamental wavelength. The generated second harmonic light at 953.5 nm was detected by a photomultiplier and referenced to quartz with $\chi_{111}^{(2)} = 0.554$ pm V^{-1} at 1907 nm.[24] For the measurement of the nonlinear optical susceptibility $\chi_{111}^{(2)}$ of DSTMS, polished *c* plates were used with the dielectric x_1 axes oriented along the rotation axis of the Maker Fringe experiment. We obtained a value of $\chi_{111}^{(2)} = (430 \pm 40)$ pm V^{-1}, which is comparable with the one of DAST $\chi_{111}^{(2)} = (420 \pm 110)$ pm V^{-1}.[24]

The nonlinear optical properties of DAST and DSTMS can be also compared by relating microscopic first-order hyperpolarizability tensor β_{xyz} with the macroscopic second order nonlinear optical susceptibility tensor $\chi_{ijk}^{(2)}$.[4] By applying the simple oriented-gas model and considering only the largest optical hyperpolarizability element β_{zzz} for generating second-harmonic light at frequency 2ω we obtain[4]

$$\chi_{111}^{(2)}(-2\omega,\omega,\omega) = N f_1^{2\omega}(f_1^{\omega})^2 \cos^3(\theta_{1z}) \cdot \beta_{zzz}(-2\omega,\omega,\omega) \qquad (2)$$

where N is the number of chromophores per unit volume, $f_1^{\omega,2\omega}$ are the local field corrections, and θ_{1z} is the angle between the polar axis 1 in the crystal and the molecular axis z of the chromopore. This angle is for DSTMS about $\theta_{1z}^{DSTMS} = 23°$ (see Fig. 3), which is slightly larger than the reported $\theta_{1z}^{DAST} = 20°$ of DAST. Assuming similar hyperpolarizabilities β_{zzz} in the solid state of DAST and DSTMS due to the same nonlinear optical active chromophore, similar local field corrections, and taking into account the change of the angle θ_{1z} and the volume of the unit cell (see Table 1), we can estimate the ratio $\chi_{111}^{(2)}(\text{DSTMS})/\chi_{111}^{(2)}(\text{DAST}) = 0.9$. The measured nonlinear optical susceptibility is however higher, which can be attributed to a decreased influence of the intermolecular interactions that are decreasing the first hyperpolarizability in the solid state of ionic compounds, due to the larger distance between the chromophores in DSTMS compared to DAST.

2.5. THz Generation

Recently, the science and technology on ultrashort electromagnetic pulses with a spectral content in the 0.1 to 10 THz range (THz pulses) have attracted widespread interest and evolved into a useful tool for a number of applications.[25–28] For example, highly efficient generation and detection of few cycle THz pulses using laser pulses at a telecommunication wavelength of 1.5 μm and DAST crystals has been demonstrated.[29] Attracted by the high nonlinear optical properties, THz

generation with DSTMS has been explored by our group. First very promising results are shown in Figure 6. We were able to demonstrate a highly efficient THz wave emission using optical rectification in a 0.34 mm thick DSTMS crystal with THz electric field strengths of more than 4 kV cm^{-1} and a frequency range of more than 4 THz. As a fundamental optical wave we used pulses at 1450 nm with a duration of 160 fs and pulse energy of 30 μJ from an optical parametric generator pumped by an amplified Ti:Sapphire laser. The generated THz wave amplitude was detected using electro-optical sampling with probe pulses at 725 nm with a 0.5 mm thick ZnTe crystal. The efficiency of THz generation in DSTMS is comparable to DAST under same conditions.[30] A characteristic phonon absorption is observed in both DAST and DSTMS close to 1 THz (see Fig. 6, right).

The generated THz amplitude scales with the material figure of merit $\chi^{(2)}/n^2$, where $\chi^{((2)}$ is the second-order nonlinear optical susceptibility and n the refractive index. Compared to the conventional inorganic ZnTe crystal, which is widely used to generate THz waves by optical rectification with $\chi^{(2)}/n^2$ of about 15 pm V^{-1}, DSTMS shows an eight times improved figure of merit of about 120 pm V^{-1}.

3. Conclusion

In summary, a novel stilbazolium salt DSTMS has been prepared from metathesis reaction. With a noncentrosymmetric crystal packing monoclinic space group *Cc*, DSTMS shows a much higher solubility in methanol and much better growth characteristics than DAST. By carefully controlling the crystal growth conditions we were able to obtain very large bulk single crystals and thin films with good optical quality without using seed crystals. Nonlinear optical measurement revealed that DSTMS possesses large nonlinear optical susceptibilities with $\chi_{111}{}^{(2)} = (430 \pm 40)$ pm V^{-1} at 1.9 μm. Highly efficient generation of THz pulses with THz electric field strengths of more than 4 kV cm^{-1} using laser pulses at a wavelength of 1.45 μm and DSTMS crystals has been demonstrated. This material is therefore very promising for second-order nonlinear optical applications such as electro-optics, frequency conversion into the Mid IR and THz generation.

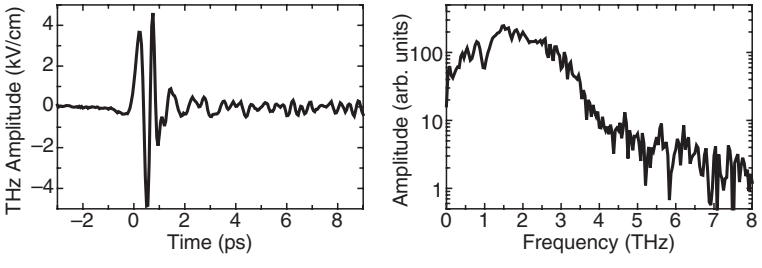

Figure 6. THz amplitude generated through optical rectification of 160 fs pulses at 1.45 μm in a 0.34 mm thick DSTMS crystal, as detected by electro-optic sampling in a 0.5 mm thick ZnTe crystal using a frequency doubled probe beam at 0.725 μm (left) and its Fourier transform (right). The oscillations for $t > 2$ ps are due to ambient water vapor absorption.

4. Experimental

Synthesis. General Considerations: All reagents were purchased as high purity (AR grade) from Aldrich and used without further purification. Stilbazolium salt was obtained by condensation reaction between 4-methyl-*N*-methyl pyridinium iodide, which was prepared from 4-picoline and methyl iodide, and 4-*N*, *N*-dimethylamino-benzaldehyde in the presence of piperidine [18]. The obtained salt was then metathesized to 2,4,6-trimethyl-benzenesulfonate by precipitation from water solution of sodium salt of 2,4,6-trimethylbenzenesulfonic acid. The products were dried in vacuum for 24 h to remove solvents effectively. ^{1}H-NMR spectra were recorded on a Brucker 300 MHz spectrometer on DMSO-d_6 solutions. Elemental analyses were performed by the Microanalytical Laboratory, ETH. Thermal analysis was conducted on a Perkin-Elmer TGA-7 and DSC-7 spectrometer at a heating rate of 10 °C min^{-1}, respectively.

4-N,N-dimethylamino-4′-N′-methyl-stilbazolium 2,4,6-trimetheylbenzenesulfonate, DSTMS: Yield 86 %; ^{1}H-NMR (300 MHz, DMSO-d_6): $\delta = 8.69$ (d, 2H, $J = 6.6$ Hz, C_5H_4N), 8.04 (d, 2H, $J = 6.6$ Hz, C_5H_4N), 7.93 (d, 1H, $J = 16.2$ Hz, CH), 7.60 (d, 2H, $J = 8.7$ Hz, C_6H_4), 7.19 (d, 1H, $J = 16.2$ Hz, CH), 6.80 (d, 2H, $J = 8.7$ Hz, C_6H_4), 6.73 (s, 2H, $C_6H_4SO_3^-$), 4.17 (s, 3H, NMe), 3.02 (s, 6H, NMe), 2.49 (s, 6H, 2Me), 2.16 (s, 3H, Me). C, H, N analysis calcd. for $C_{25}H_{30}N_2O_3S$: C 68.46, H 6.89, N 6.39; found: C 68.42, H 6.85, N 6.36.

X-Ray Crystallography: The crystal structures were measured on X-ray diffractometers equipped with CCD detectors, solved and refined with SHELX. For details see the deposited material. CCDC-277597 contains the supplementary crystallographic data for this paper. These data can be obtained free of charge from The Cambridge Crystallographic Data Centre via www.ccdc.cam.ac.uk/data_request/cif

Received: November 21, 2006
Revised: March 3, 2007
Published online: August 2, 2007

[1] *Nonlinear Optical Properties of Organic Molecules and Crystals*, Vols. 1 and 2 (Eds: D. S. Chemla, J. Zyss), Academic, Orlando, FL **1987**.

[2] *Materials for Nonlinear Optics: Chemical Perspective* (Eds: S. R. Marder, J. E. Sohn, J. D. Stucky), ACS Symposium Series, Vol. 455, ACS, Washington, DC **1991**.

[3] C. Bosshard, K. Sutter, P. Prêtre, J. Hulliger, M. Flörsheimer, P. Kaatz, P. Günter, *Organic Nonlinear Optical Materials*, Gordon and Breach, Amsterdam **1995**.

[4] C. Bosshard, M. Bösch, I. Liakatas, M. Jäger, P. Günter, in *Nonlinear Optical Effects and Materials* (Ed: P. Günter), Springer, New York **2000**, Ch. 3.

[5] A. Schneider, I. Biaggio, P. Günter, *Appl. Phys. Lett.* **2004**, *84*, 2229.

[6] S. R. Marder, J. W. Perry, *Science* **1994**, *263*, 1706.

[7] *Molecular Nonlinear Optics: Materials, Physics, and Devices* (Ed: J. Zyss), Academic, New York **1994**.

[8] G. R. Meredith, in *Nonlinear Optical Properties of Organic and Polymeric Materials* (Ed: D. J. Williams), ACS Symp. Series, Vol. 233, ACS, Washington, DC **1983**, pp. 27–56.

[9] B. J. Coe, J. A. Harris, I. Asselberghs, K. Wostyn, K. Clays, A. Persoons, B. S. Brunschwig, S. J. Coles, T. Gelbrich, M. E. Light, M. B. Hursthouse, K. Nakatani, *Adv. Funct. Mater.* **2003**, *13*, 347.

[10] S. R. Marder, J. W. Perry, W. P. Schaefer, *Science* **1989**, *245*, 626.

[11] F. Pan, M. S. Wong, C. Bosshard, P. Günter, *Adv. Mater.* **1996**, *8*, 592.

[12] P. Lavéant, C. Medrano, B. Ruiz, P. Günter, *Chimia* **2003**, *57*, 1.

[13] Y. Hosokawa, H. Adachi, M. Yoshimura, Y. Mori, T. Sasaki, H. Masuhara, *Cryst. Growth Des.* **2005**, *5*, 861.

ADVANCED FUNCTIONAL MATERIALS

[14] Y. kaneko, S. Shimada, T. Fukuda, T. Kimura, H. Yokoi, H. Matsuda, T. Onodera, H. Kasai, S. Okada, H. Oikawa, H. Nakanishi, *Adv. Mater.* **2005**, *17*, 160.
[15] R. M. Kumar, D. R. Babu, G. Ravi, R. Jayavel, *J. Cryst. Growth* **2003**, *250*, 113.
[16] S. Manetta, M. Ehrensperger, C. Bosshard, P. Günter, *C. R. Phys.* **2002**, *3*, 449.
[17] H. Umezawa, K. Tsuji, Anwar, X.-M. Duan, S. Okada, H. Oikawa, H. Matsuda, H. Nakanishi, *MCLC S&T, Sect. B: Nonlinear Opt.* **2000**, *24*, 73.
[18] S. R. Marder, J. W. Perry, C. P. Yakymyshyn, *Chem. Mater.* **1994**, *6*, 1137.
[19] S. Okada, K. Nogi, Anwar, K. Tsuji, X.-M. Duan, H. Oikawa, H. Matsuda, H. Nakanishi, *Jpn. J. Appl. Phys. Part 1* **2003**, *42*, 668.
[20] Z. Yang, S. Aravazhi, A. Schneider, P. Seiler, M. Jazbinsek, P. Günter, *Adv. Funct. Mater.* **2005**, *15*, 1072.
[21] B. Ruiz, Z. Yang, V. Gramlich, M. Jazbinsek, P. Günter, *J. Mater. Chem.* **2006**, *16*, 2839.
[22] J. C. Brice, *Crystal Growth Process*, Wiley, New York **1996**.
[23] J. Jerphagnon, S. K. Kurtz, *J. Appl. Phys.* **1970**, *41*, 1667.
[24] U. Meier, M. Bösch, C. Bosshard, F. Pan, P. Günter, *J. Appl. Phys.* **1998**, *83*, 3486.
[25] B. Ferguson, X.-C. Zhang, *Nat. Mater.* **2002**, *1*, 26.
[26] S. Brahadeeswaran, S. Onduka, M. Takagi, Y. Takahashi, H. Adachi, M. Yoshimura, Y. Mori, T. Sasaki, *J. Cryst. Growth* **2006**, *292*, 441.
[27] Y. Takahashi, H. Adachi, T. Taniuchi, M. Takagi, Y. Hosokawa, S. Onzuka, S. Brahadeeswaran, M. Yoshimura, Y. Mori, H. Masuhara, T. Sasaki, H. Nakanishi, *J. Photochem. Photobiol. A* **2006**, *183*, 247.
[28] H. Adachi, T. Taniuchi, M. Yoshimura, S. Brahadeeswaran, T. Higo, M. Takagi, Y. Mori, T. Sasaki, H. Nakanishi, *Jpn. J. Appl. Phys. Part 1* **2004**, *43*, L1121.
[29] A.Schneider, M. Stillhart, P. Günter, *Opt. Express* **2006**, *14*, 5376.
[30] A. Schneider, M. Neis, M. Stillhart, B. Ruiz, R. U. A. Khan, P. Günter, *J. Opt. Soc. Am. B* **2006**, *23*, 1822.